

Texture Camera System with Self-calibration for Use Aboard UAVs



Feifei Xie¹, Zongjian Lin², and Guozhong Su²

¹ State Key Laboratory of Mining Disaster Prevention and Control Co-founded by Shandong Province and the Ministry of Science and Technology, Shandong University of Science and Technology, 579 Qianwangang Road, Qingdao, China
xiefeifei_007@163.com

² Chinese Academy of Surveying and Mapping, 16 Beitaping Road, Beijing, China
lincasm@casm.ac.cn

Received 9 November 2015; Revised 12 February 2016; Accepted 7 April 2016

Abstract. Because of their excessive weight, currently available oblique cameras are not suitable for use aboard a low-altitude unmanned aerial vehicle (UAV) with a light load. In this study, a texture camera system for use aboard a UAV is designed, and it can simultaneously obtain a single vertical image and four oblique images of an object. The images acquired by this self-calibrating camera system can be used to perform traditional products on a large scale. Additionally, they can be used to accurately determine the orientation elements of each individual camera, which are essential for three-dimensional (3D) modeling. Finally, typical engineering data is used to verify the given theoretical analysis. We conclude that the mosaic images obtained by the proposed texture camera system aboard the UAV meet the precision requirements of an aerial survey topographic map with a scale of 1:500 and the building facade textures are complete and clear. Using this texture camera system, 3D building models with a high mapping accuracy and realistic textures can be established.

Keywords: 3D modeling, self calibration, mapping accuracy, oblique photography, UAV

1 Introduction

With the need for city planning, landscape architectural design, 3D navigation applications on real 3D city landscape, the establishment of 3D city models with real building images will have a higher economic value and application prospect. How to economy, rapidly acquire the 3D building model data, especially the fast acquisition of building texture data has not been solved well. Now, it relies on the manual operation to complete. And the manpower cost of this process is high, which has become a “bottleneck” for establishing real 3D city model.

In recent years, a new technology named oblique photography technology is developed in the international geographic information field [1]. The multi sensor integration mechanism is used for oblique photography technology, including a new multi line (surface) array, multi angle digital cameras, such as three line array camera system ADS40/80, the three camera system AOS, the four camera system UCD and DMC, the five camera system Pictometry Camera and Chinese SWDC-5, AMC580, TOPDC-5 etc. [2-7]. These cameras can obtain the vertical image and four oblique images of an object at a time, which overcomes the traditional aerial technology only obtaining images from the vertical angle. According to the advanced positioning technology and processed method, such as the oblique image processing software Pictometry, Street Factory system, MultiVision system etc., the 3D geometric information and rich texture information can be obtained [8-19].

The flying platform of oblique photography technology is most the manned aircraft, the disadvantage of which are high cost, poor safety, low time resolution and building obscure in the image. In recent

years, low altitude unmanned aerial system (UAVS) is developing very fast, which makes up the shortage of satellite remote sensing and high altitude aerial in timeliness and precision aspects [20]. But the oblique camera systems on the market are not suitable for the low altitude UAV [21-24]. The reasons are shown as bellow.

Firstly, these oblique camera systems can not do self calibration. The self calibration refers to the rotary variable $\Delta \omega$, $\Delta \varphi$ and $\Delta \kappa$ of every camera relative to other cameras can be found and detected through the overlapping area between any of the camera [25]. For example, the cameras UCD and DMC use a few small cameras with a certain distance, and the images of each small cameras are uptake into a large format image. Because of the small overlap between the small cameras, when the camera rotates around the X axis or Y axis, the self calibration condition can not be found. It leads to the big image distortion, which means the image quality is low.

Secondly, the total weight of the oblique camera systems on the market is mostly over 100kg, which is not suitable for UAV with a light load. In order to improve the images quality without self calibration, the mechanical structure is used to reinforce the connection piece, and the relative position and the dip angle of the single camera are kept unchanged at the same time. So the weight of the camera system is over 100kg. But the maximum task of UAV such as the unmanned airship is not more than 20kg, it is difficult to carry this camera system.

Finally, the camera's field of view is limited. The camera DMC can get the maximum image 8000 x 14000 pixels, the camera focal length 120mm, but the view angle is only $69.3^\circ \times 42^\circ$. Lin (2012) has developed the 4 combined wide-angle digital camera aboard the unmanned airship, which can overcome the low operating efficiency and meet the 1:500 scale aerial survey precision [26]. But this camera is designed only for realizing low altitude mapping with large scale, and the tilt angle of every camera is small, which cannot fully meet the demand of the data source for 3D city modeling.

The objective of this research, therefore, is to design a five combined wide-angle digital camera named as texture cameras, which can be aboard on UAV for 3D city modeling. Two kinds design schemes and working principle of texture camera are introduced, especially the self calibration technology is researched to composite imaging static error and dynamic error. Compared with the existing oblique photography methods, texture camera system aboard on UAV has the superiority in flexibility, cost and accuracy.

2 Texture Camera System

Texture camera model is designed as showed in Fig. 1. Five single cameras A, B, C, D, and E are fixed on the stable platform, and there is a certain degree of overlapping between the adjacent cameras. Without loss of generality, two kinds of SLR cameras as the focal length 24mm, field angle $72.7^\circ \times 51.9^\circ$ degrees and the focal length 35mm, field angle $51.9^\circ \times 37.8^\circ$ degrees are selected as the single camera for texture camera system.

The spatial coordinate system XYZ is set up, in which the XY plane is the horizontal plane, and the Z axis coinciding with texture camera center is pointing to the zenith direction. The center of camera E is set on the origin of coordinate system XYZ, of which the long side is parallel to the X axis, and the short side parallel to the Y axis. Camera C and D are symmetrically arranged with the origin in the Y axis, of which the main axis is respectively tilt ω angle relative to the Z axis. It means that these two cameras only do an equal amount of relative rotate around X axis, which is shown in Fig. 2. Half of the view angle with the long side of single camera is θ , whose view angle relative to the Y axis is $2\theta + 2\omega$. Similarly, camera A and B are symmetrically arranged with the origin in the X axis. In the long side direction of the camera, the overlap between camera E with the adjacent camera is 18 degrees (see Fig. 2(a)). In the short side direction of the camera, the overlap is 7 degrees (see Fig. 2(b)). So there is sufficient overlap to do self calibration.

Considering the economic cost and the total pixels, Cannon EOS 5D MarkII camera is chosen for texture camera system, whose basic parameters is shown in Table 1. Table 2 is the performance parameter of texture camera system.

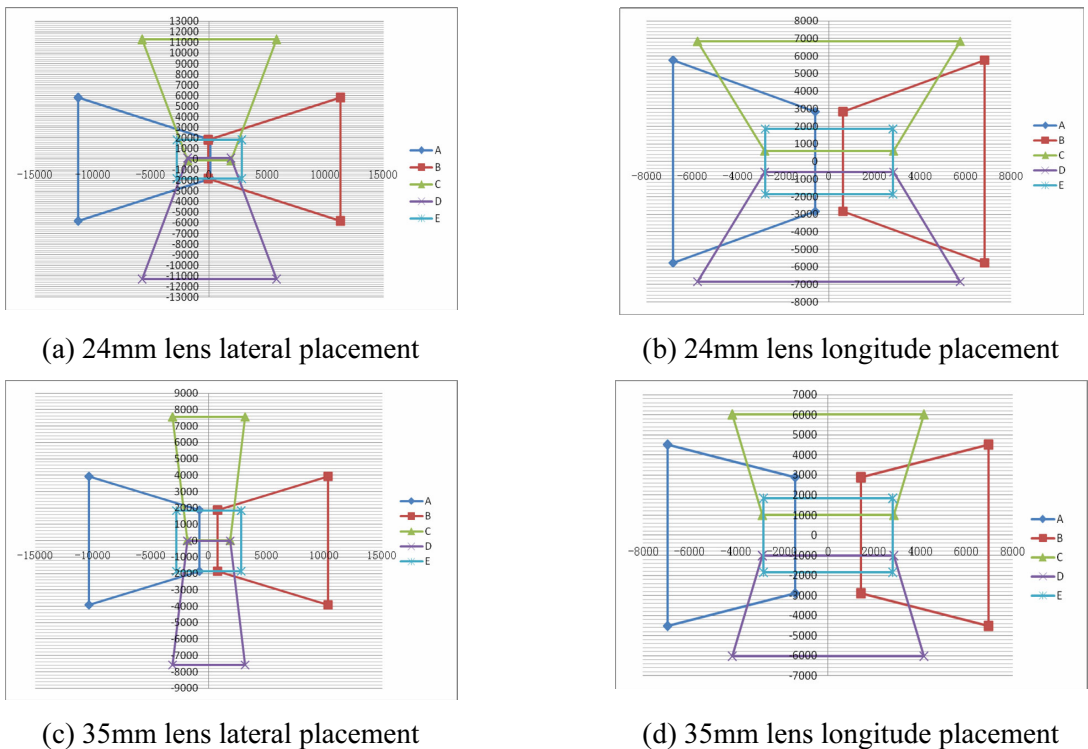


Fig. 1. The model design of texture camera

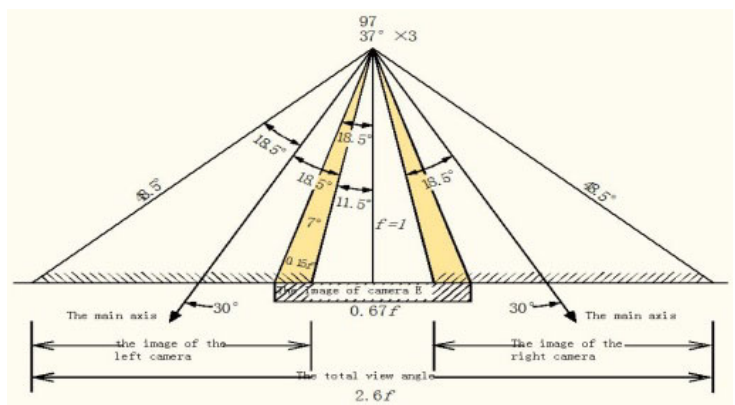
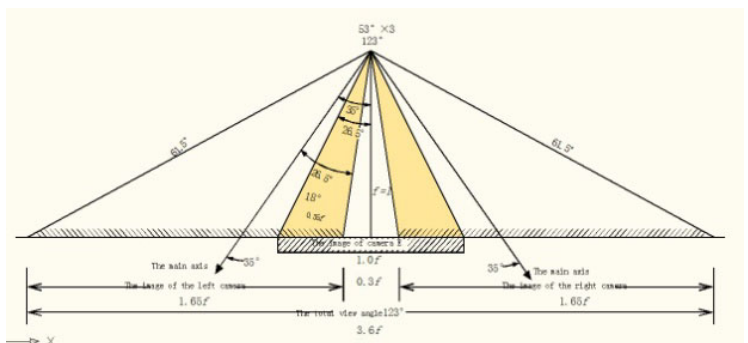


Fig. 2. The three adjacent cameras imaging profile

Table 1. The performance parameter of Canon EOS 5D MarkII camera

Frame (pixel)	CCD size (μ)	Viewing angle (degree)	Price (RMB)	Weight (g)
5616×3744	6.3	72.7×51.9	22000	810

Table 2. The performance parameters of texture camera

Focal lens (mm)	Max resolution (pixel)	Viewing angle (degree)	Camera tilt angle (degree)	CCD size (μ)
24(lateral)	22562×22562	142×142	35×35	6.3
24(longitude)	13686×13686	121×121	35×35	6.3
35(lateral)	20672×15134	123×107	27×35	6.3
35(longitude)	13884×12052	103×95	29×33	6.3

The designed texture camera, using five cameras combine with big tile angle, can obtain clear building images from a vertical and four oblique angles at a time. At the same time, the big viewing angle contributes to the likelihood of high aerial survey precision.

3 Self Calibration of Texture Camera

The work process of the existing oblique photography sensor is generally the same. Firstly, the relative orientation elements of the combination camera are gotten by the ground static calibration, including each single camera field calibration and the combination camera relative orientation calibration. Secondly, the mechanical structure is used to rigidly connect each single camera to achieve the relative elements stability. At the same time, the synchronous exposure device is used to control each single camera synchronous exposure at the same station. Finally, image orientation elements of each single camera can be calculated by the high precision record system. Although the images with big oblique angles can be obtained by the sensor with strong optical mechanical design, the total weight is over 100kg, which is not suitable for the small UAV with safety and low altitude flight. In order to meet the light load demand for small UAV, on the one hand the lightweight materials can be used for camera frame, which will generate mechanical deformation with each imaging. On the other hand, the actual aerial is motion process, which will tend to produce dynamic imaging error by the exposure delay between single cameras. Because of these factors, each single camera positioning precision becomes low.

So, texture camera aboard on UAV is designed, which can achieve self calibration by the image overlapping area and overcome static mechanical error and dynamic imaging error. Two aspects of application are supported by texture camera. On the one hand, the mosaic image of one equivalent single center can be obtained by a mosaic with five single cameras, which can be used for aerial triangulation to realize the large scale mapping. On the other hand, according to the relationship between single cameras and the mosaic image, the exact orientation elements of each single camera are calculated by the orientation elements of the mosaic image, which can be used for 3D modeling (see Fig. 3).

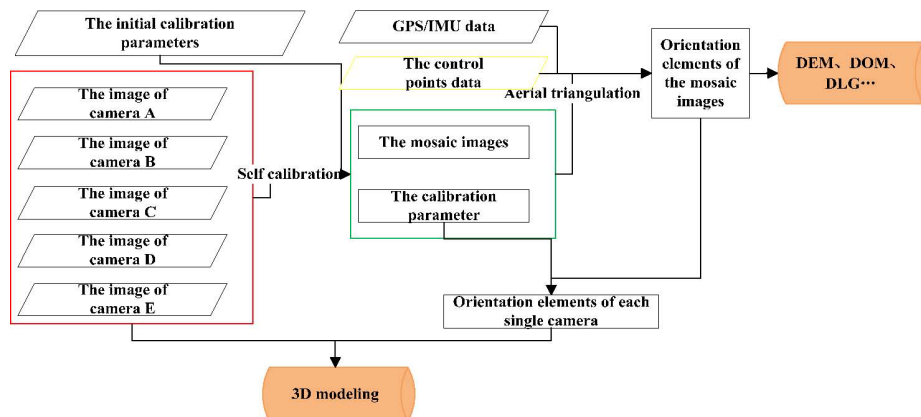


Fig. 3. The operation flow chart of texture camera

3.1 The Process of Self Calibration

The paper size is A4. The printing margins are: 2cm for up and down margins and 2.5cm for left and right margins. The text should be justified to occupy the full line width, so that the right margin is not ragged, with words hyphenated as appropriate.

Self calibration of texture camera refers to detect the change of images coordinates by the overlap between single cameras, and building the error equation with the principle of the same points in the same location in the available error range. Finally, the position relationship between single cameras with high precision is calibrated and the mosaic image is generated. The process is as follows:

- (1) The definition of the respective image plane coordinates system of five single cameras.
- (2) The definition of the image plane coordinates system of the mosaic image.
- (3) Sampling to generate five level images from five single cameras.
- (4) Calculating the dividing line in the overlapping area between the five level images.
- (5) Points matching (the overlapping areas AE, BE, CE and DE used for self calibration are shown in Fig. 4).

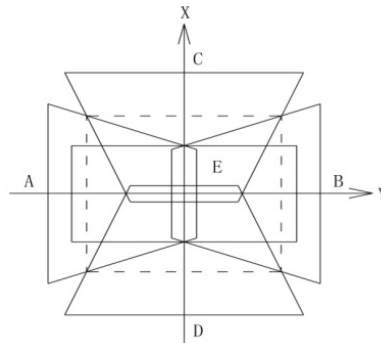


Fig. 4. The overlapping area for self calibration

- (6) Building the error equation with the principle of the same points in the same location in the available error range.

- (7) Calculating the error equation to detect the attitude angle change of each camera and obtain the uniform correction parameters.

- (8) Generating the mosaic images of the correction parameters in every exposure.
- (9) Dodging the mosaic images.

The calibration process of texture camera with self calibration is shown as Fig. 5.

Because the aerial photogrammetry is a dynamic process, the relationship between single cameras is constantly changing during the flight. So the calibration process of texture camera with self calibration is done in every exposure to detect each single camera pose changes caused by platform motion and avoid frequent field camera calibration. After self calibration the accurate relative exterior orientation relationship of texture camera is built.

3.2 Self calibration for Static Error

The self calibration for static error refers to the mosaic image stitching not directly using the field calibration value but further correcting according to the images overlap between single cameras to archive the strict conversion for one single center projection and splicing.

According to the collinearity condition and transformation between coordinate systems, the coordinate's values of A, B, C, D and E cameras are shown as equation (1), (2), (3), (4) and (5).

$$\begin{bmatrix} X \\ Y \\ -f \end{bmatrix}_A = \begin{bmatrix} 1 & 0 & 0 \\ 0 & \cos \omega & -\sin \omega \\ 0 & \sin \omega & \cos \omega \end{bmatrix} \begin{bmatrix} x \\ y \\ -f \end{bmatrix}_A + \begin{bmatrix} S_x \\ S_y \\ S_z \end{bmatrix}_A, \quad (1)$$

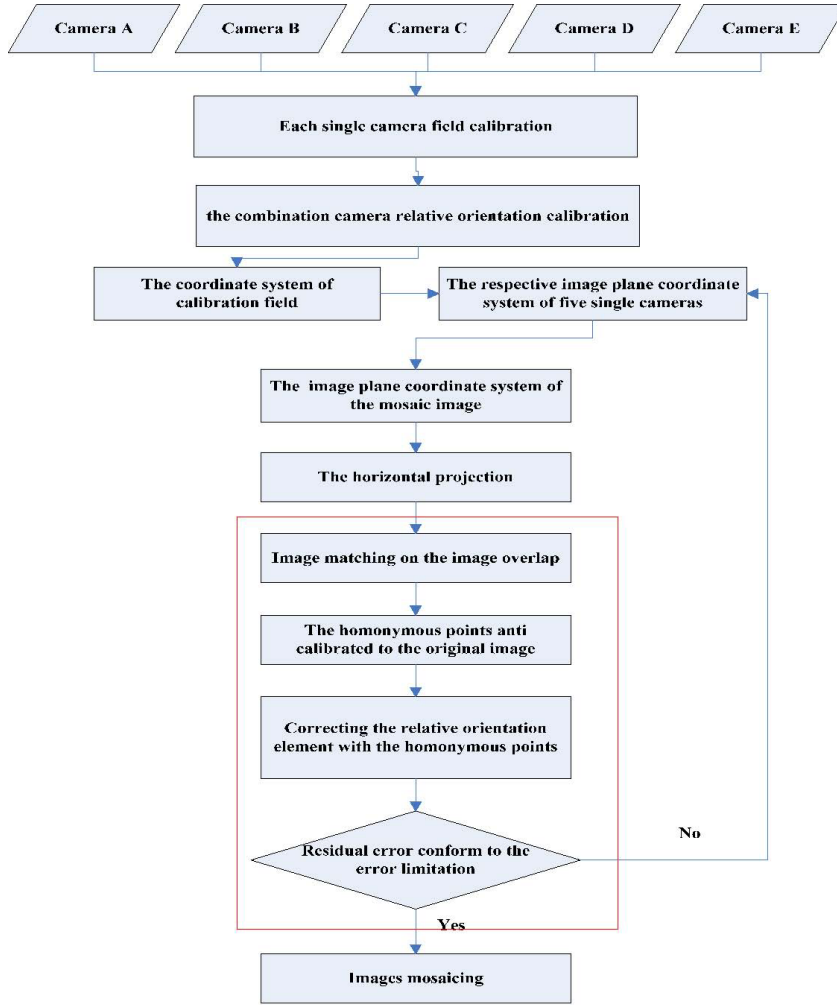


Fig. 5. The calibration process of texture camera with self calibration

$$\begin{bmatrix} X \\ Y \\ -f \end{bmatrix}_B = \begin{bmatrix} 1 & 0 & 0 \\ 0 & \cos \omega & \sin \omega \\ 0 & -\sin \omega & \cos \omega \end{bmatrix} \begin{bmatrix} x \\ y \\ -f \end{bmatrix}_B + \begin{bmatrix} S_x \\ S_y \\ S_z \end{bmatrix}_B \quad (2)$$

$$\begin{bmatrix} X \\ Y \\ -f \end{bmatrix}_C = \begin{bmatrix} \cos \varphi & 0 & -\sin \varphi \\ 0 & 1 & 0 \\ \sin \varphi & 0 & \cos \varphi \end{bmatrix} \begin{bmatrix} x \\ y \\ -f \end{bmatrix}_C + \begin{bmatrix} S_x \\ S_y \\ S_z \end{bmatrix}_C \quad (3)$$

$$\begin{bmatrix} X \\ Y \\ -f \end{bmatrix}_D = \begin{bmatrix} \cos \varphi & 0 & \sin \varphi \\ 0 & 1 & 0 \\ -\sin \varphi & 0 & \cos \varphi \end{bmatrix} \begin{bmatrix} x \\ y \\ -f \end{bmatrix}_D + \begin{bmatrix} S_x \\ S_y \\ S_z \end{bmatrix}_D \quad (4)$$

$$\begin{bmatrix} X \\ Y \\ -f \end{bmatrix}_E = \begin{bmatrix} 1 & 0 & 0 \\ 0 & 1 & 0 \\ 0 & 0 & 1 \end{bmatrix} \begin{bmatrix} x \\ y \\ -f \end{bmatrix}_E + \begin{bmatrix} S_x \\ S_y \\ S_z \end{bmatrix}_E \quad (5)$$

Equation (1), (2), (3), (4) and (5) can be simplified to equation (6).

$$\begin{bmatrix} \bar{X} \\ \bar{Y} \\ -f \end{bmatrix} = \begin{bmatrix} a_{i1} & a_{i2} & a_{i3} \\ b_{i1} & b_{i2} & b_{i3} \\ c_{i1} & c_{i2} & c_{i3} \end{bmatrix} \begin{bmatrix} x \\ y \\ -f \end{bmatrix} + \begin{bmatrix} S_x \\ S_y \\ S_z \end{bmatrix} \quad (6)$$

Where $[S_x S_y S_z]_{T_i}$ are the coordinates of center of A, B, C, D and E cameras, a_i , b_i and c_i are the direction cosine matrix for the angle elements ω , φ and κ .

According to the overlapping area between adjacent level images that are gotten from each single camera image projected to the horizontal coordinate, the image parallax error Δx_{ij} and Δy_{ij} are detected by image matching method. Then the incremental changes of the relative orientation elements ΔS_x , ΔS_y , ΔS_z , $\Delta \omega$, $\Delta \varphi$ and $\Delta \kappa$ are solved by the equation (7).

$$\begin{cases} \Delta x_{ij} = \Delta S_{x_{ij}} + \frac{x}{f} \Delta S_{z_{ij}} + f \left(1 + \frac{x^2}{f^2} \right) \Delta \varphi_{ij} + \frac{xy}{f} \Delta \omega_{ij} - y \Delta \kappa_{ij} \\ \Delta y_{ij} = \Delta S_{y_{ij}} + \frac{y}{f} \Delta S_{z_{ij}} + \frac{xy}{f} \Delta \varphi_{ij} + f \left(1 + \frac{y^2}{f^2} \right) \Delta \omega_{ij} + x \Delta \kappa_{ij} \end{cases} \quad (7)$$

Where f is the principal distance, i and j are the adjacent image numbers.

3.3 Self Calibration for Dynamic Error

The synchronous error of camera exposure is a random error and exists objectively, which leads to the existence of a certain number of exposure delay between single cameras. Finally, there will be a fine-tuning on the relative orientation relationship of images obtained from single cameras at one exposure time. In order to detect and correct the dynamic error, the motion equation of the camera orientation elements (equation (8)) and the relation model between parallax error and the camera orientation elements (equation (9)) are used to calibrate the dynamic incremental of the orientation elements and correct the dynamic error of images.

$$\begin{bmatrix} d\Delta S_{x_i} \\ d\Delta S_{y_i} \\ d\Delta S_{z_i} \\ d\Delta \varphi_i \\ d\Delta \omega_i \\ d\Delta \kappa_i \end{bmatrix} = \Delta T_i \begin{bmatrix} VS_{x_i} \\ VS_{y_i} \\ VS_{z_i} \\ V\varphi_i \\ V\omega_i \\ V\kappa_i \end{bmatrix} + \begin{bmatrix} QS_{x_i} \\ QS_{y_i} \\ QS_{z_i} \\ Q\varphi_i \\ Q\omega_i \\ Q\kappa_i \end{bmatrix} \quad (8)$$

$$P(\Delta x_{ij}, \Delta y_{ij}) = F(\Delta S_{x_i}, \Delta S_{y_i}, \Delta S_{z_i}, \Delta \varphi_i, \Delta \omega_i, \Delta \kappa_i, \Delta S_{x_j}, \Delta S_{y_j}, \Delta S_{z_j}, \Delta \varphi_j, \Delta \omega_j, \Delta \kappa_j) \quad (9)$$

Where $(\Delta S_{x_i}, \Delta S_{y_i}, \Delta S_{z_i}, \Delta \varphi_i, \Delta \omega_i, \Delta \kappa_i)$ is the increment of the azimuth element of the camera i , Q is the corresponding initial value, V is the corresponding motion velocity, ΔT_i is the corresponding delay of the camera exposure time, $(\Delta x_{ij}, \Delta y_{ij})$ are the parallax errors of the overlap between images i and j .

Firstly, the parallax error equation (equation (7)) is built by the corresponding image points which are gotten by image matching on the overlapping area between single camera images. Then, the relative control condition that texture camera system has a unified coordinate system is used as equation (10). Combined with the equation (7), (8), (9) and (10) for overall adjustment, the orientation elements of each single camera image can be calculated accurately, with which the accurate conversion from five single images to a mosaic image with one single projection center is realized.

$$\left. \begin{aligned} \Delta\omega_A + \Delta\omega_B + \Delta\omega_C + \Delta\omega_D &= 0 \\ \Delta\varphi_A + \Delta\varphi_B + \Delta\varphi_C + \Delta\varphi_D &= 0 \\ \Delta\kappa_A + \Delta\kappa_B + \Delta\kappa_C + \Delta\kappa_D &= 0 \end{aligned} \right\} \quad (10)$$

3.4 Large overlap of low altitude aerial with Texture Camera System

In addition to use the texture camera system to improve image geometric quality, the operation of large overlap can be use to improve accuracy of low altitude photogrammetry. According to the analysis of photogrammetry, in order to improve the accuracy of low altitude photogrammetry, the wide angle camera muse be used. But the mapping accuracy is not uniform in one stereo image pair with high accuracy on the center and low accuracy on the edge. So if the middle of images is used for mapping (including DEM, DOM and DLG), it can get high accuracy. The actual practice is increasing the image overlap. For example, the longitudinal overlap degree is 80%, and side overlap is 60%. For digital camera, the work efficiency is not reduced by increasing the longitudinal overlap. Need to pay operating cost is only the side overlap increase. But compared with the accuracy of the results improvement, its price is cost-effective.

4 Test and Aanalysis

4.1 The Test Plan

The image data of Yuncheng city, Shanxi Province in China is selected as the test data, with the area of 65 square kilometers. Yuncheng city is a relatively dense population and has many styles of buildings, which are suitable for verifying the feasibility of high safety and fast 3D city modeling method with texture camera system aboard on UAV. The aerial sensor is texture camera shown in Fig. 6, with total weight of 15.6kg. The aerial platform is the unmanned airship CK-FT180 shown in Fig. 7, with a high frequency GPS. According to the requirement of aerial mission with 1:500 flight scale, the specific parameters of the route plan are shown in Table 3.



Fig. 6. Texture camera



Fig. 7. The unmanned airship CK-FT180

Table 3. The parameters of route plan

Focal length (mm)	CCD size (u)	View angle (degree)	Image format (pixel)	Flying height (m)	Ground resolution (m)	Side over-lap (%)	Longitudinal overlap (%)
35	6.3*6.3	103*95	12000*13000	240	0.045	60	80

4.2 The Imaging Quality and Self Calibration Accuracy

A frame of images from texture camera system aboard on unmanned airship is shown in Fig. 8, including the images of each single camera and mosaic image. From the Fig. 8, we can see that a complete building façade texture can be obtained by the single oblique camera, and the mosaic image does not exist obvious deviation and seam, even zoomed to the actual pixel.

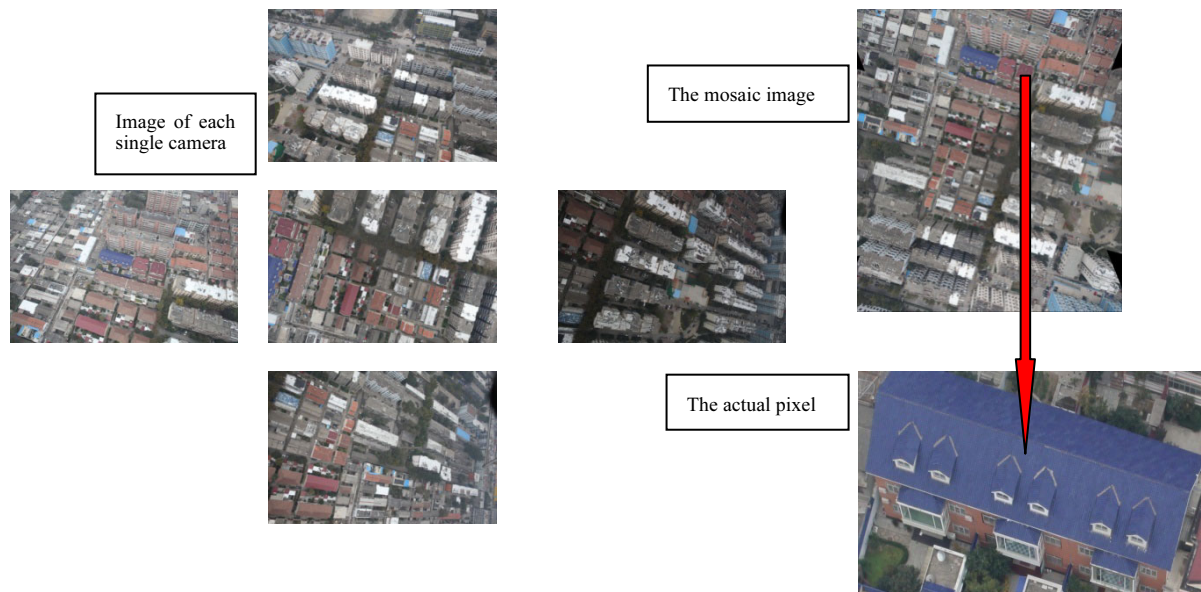


Fig. 8. Images of texture camera

The parameters of lens distortion, plane distortion and the position relation of the five single cameras are calibrated by outdoor field, which is used to correct part of a system error in the process of aerial photograph. But geometric distortion caused by curtain shutter and asynchronous control factors is modified by the self calibration technology. The experiments are done as follows. Table 4 shows that the static distortion caused by the imaging unit is up to more than 13 pixels, but after error calibration, the stitching error can be controlled within 0.2 pixels. Table 5 shows that just considering the timing control, distortion caused by motion is likely to reach more than 20 pixels, but after self calibration, the error can be controlled within 0.5 pixels. The distortion of the wide angle mosaic image can be controlled within 1 pixel after the static and dynamic calibrations. It means that relative orientation accuracy of each single camera is high by self calibration.

Table 4. The camera accuracy table with static ground calibration field (pixel)

Matching area ID	The residuals before self-calibration	The residuals after self-calibration	Error before self calibration	Error after self calibration
AB	-9.0000	0.1643		
CD	-11.3000	0.1590		
AE	-13.0000	-0.0926	RMS = 7.1327	RMS = 0.1159
BE	4.7258	0.1878		
CE	9.0000	0.0145		
DE	8.0000	-0.1231		

Table 5. The camera accuracy table with dynamic calibration field

Control points ID	The residuals (m)			Pass points ID	The residuals (m)		
	Rx	Ry	Rz		Rx	Ry	Rz
112	0.008	0.001	-0.004	20000007	0.005	-0.014	0.013
113	0.006	-0.005	0.006	20000008	0.005	-0.013	0.012
114	0.005	0.001	-0.003	20000009	0.006	0.021	-0.016
115	0.012	0.004	-0.004	20000010	0.003	0.019	-0.014
...
RMS	0.010	0.007	0.008	The standards parallax error of pass points: RMS (pixel): Sigma = 0.03			

4.3 The Experiment of Relative Orientation

The actual aerial images are used to show the relationship between the field angle and relative orientation accuracy. A stereo pair of wide angle images are artificially cut into three pairs with different image field sizes (see Fig. 9). In the case of elements of exterior orientation in the same and known, the relative orientation results of three pairs of wide angle images show different accuracy (see Table 6). According to the assessment result, although three kinds of operations have eliminated the parallax error, the stereo images with big field angle can get high relative orientation precision.



Fig. 9 The images with different view angles

Table 6. The contrast of the relative orientation accuracy with different view angle

Image width (pixel)	Field view angle (°)	Points used for relative orienta- tion/matching points	Elements of relative orientation			Error of relative orientation	
			Line element (m) x	y	z	Line element (m) $m1$	Angle element (°) $m2$
			Angle element (°) φ	ω	κ		
7168	121.7	111/1365	38.313	29.937	-0.858	0.067	
			2.056	-0.864	-3.795	0.033	
4886	101.4	108/1254	38.322	29.928	-0.825	0.075	
			2.075	-0.885	-3.803	0.049	
3996	89.9	42/909	38.325	29.936	-0.821	0.072	
			2.088	-0.909	-3.808	0.064	

Note. The reference elements value of relative orientation: 38.344 30.049 -0.871 2.024 -0.8331 -3.7603.

4.4 The Aerial Triangulation Test

Ten images are selected from two flight lines, which are changed the overlaps between the images to do the aerial triangulation test. The overlaps change method is done as 4.2. With the same aerial triangulation method, the aerial triangulation result with different overlaps are shown in different accuracy (see Table 7). According to the assessment result, the stereo images with large overlap can get high aerial triangulation precision. The elevation accuracy of one object in the images with different overlaps is different, which is shown in Table 8. We can find that the points precision in the elevation direction has a great increase with the increase of the image overlap degree.

Table 7. The aerial triangulation result with different overlaps

Aerial overlap (%)	Image width/height (pixel)	The maximum residuals (m)			The average residuals (m)		
		$M_{\max x}$	$M_{\max y}$	$M_{\max z}$	M_x	M_y	M_z
80	7168/8192	0.123	0.167	0.178	0.037	0.040	0.071
70	4885/7060	0.160	0.195	0.276	0.068	0.083	0.154
60	3996/5989	0.312	0.348	0.345	0.132	0.131	0.257

Table 8. The elevation accuracy with different overlaps

Overlap degree	Intersection angle	Point ID/Elevation different (m)					
		P1	P2	P3	P4	P5	P6
2 (img436-437)	13.8°	0.056	0.087	0.119	0.082	0.09	0.074
3 (img436-438)	29.0°	0.013	0.024	0.102	0.051	0.075	0.035
4 (img436-439)	43.7°	0.011	0.007	0.024	0.024	0.05	0.017
5 (img436-440)	58.3°	0.003	0.008	0.010	0.019	0.048	0.022

The aerial triangulation experiment is done by the module MATCH-AT of digital photogrammetry software INPHO. The aerial triangulation result is shown in Table 9.

Table 9. The control point accuracy table

Flight ID	X direction residuals (m)	Y direction residuals (m)	Z direction residuals (m)
1	0.077	0.078	0.140
2	0.092	0.093	0.178
3	0.041	0.042	0.079

According to “Specifications for aerophotogrammetric office operation 1:500, 1:1000, 1:2000 topographic maps” (GB7930-87), the plane location error of 1:500 topographic maps is less than 0.4mm, that is $500 \times 0.0004\text{m} = 0.2\text{m}$. According to the standard of the plane elevation error, the ground is within 0.2m, the hilly land is within 0.35m, and the mountain is within 0.5m. After strict adjustment calculation check, the results can meet with the accuracy requirements of 1:500 mapping.

According to Table 4, Table 5 and Table 9, we can find that the orientation elements with high accuracy of every mosaic images can be obtained by aerial triangulation, which combining with the orientation elements of every single camera images by self calibration are used to provide reliable data source for 3D city modeling with high mapping accuracy.

4.5 The 3D City Modeling Test

According to the orientation elements of the mosaic images and the camera relative parameters with self calibration, the orientation elements of each single camera are calculated, which are used as the basic data for 3D building modeling. Each surface textures of one building after 3D modeling are shown in Fig. 10. From the Fig. 10, we can find that the building façade textures are clear and adjacent textures are corresponded reasonable. Traditional 3D building models are shown in Fig. 11, whose textures are selected from existing texture database and deviates from the color information of the real world. Fig. 12 is the 3D building models using texture camera system, which retain the original real scene and ornamental.

**Fig. 10.** Each surface of one building

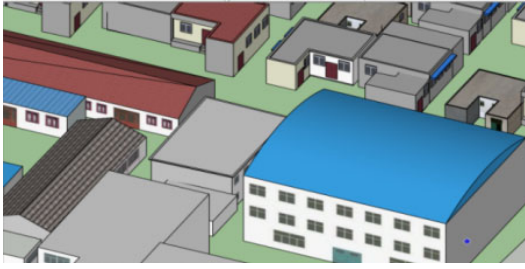


Fig. 11. The traditional 3D building models



Fig. 12. The 3D building models using texture camera system

5 Conclusion

In this paper, texture camera system with self calibration is designed aboard on UAV, which is used for aerial survey with 1:500 scale and 3D city modeling Yuncheng city. Firstly, through the actual aerial, it proves that texture camera system aboard on UAV can obtain the target building images including building roof and each facade at one time, which meets the City Building 3D modeling demand for texture images. Secondly, through aerial triangulation with the mosaic images, the result meets the accuracy requirement of 1:500 scale, which can be used for large scale aerial mapping. Thirdly, through self calibration of texture camera, the image orientation elements of each single camera are calculated with high accuracy, which can be used for 3D building modeling with high mapping accuracy to expand the 3D model economic value. Although the processes of image mosaic and aerial triangulation increase the data processing time, on the one hand, with the efficient processing technology of the computer GPU, the image mosaic speed can control an average of 15 seconds per image. On the other hand, the mosaic images can be directly used for aerial triangulation software, the technology of which is mature. Based on data acquisition efficiency, cost and accuracy, the designed texture camera system aboard on UAV for 3D city modeling will have the practical significance for economic and efficiently reconstructing building façade with real images. Especially, with the trend of “close range photogrammetry to airborne”, texture camera system also provides a viable platform for close range photogrammetry development.

The next stage of our study is to use this texture camera system for fast 3D modeling, particularly on the method of rapid extraction and optimization of the building texture.

Acknowledgement

This study was partially funded by the National Science Foundation of China (Project #41371425 and #41271451), supported by SDUST Research Fund (2014TDJH101), Joint Innovative Center for Safe And Effective Mining Technology and Equipment of Coal Resources, Shandong Province, and Scientific Research Foundation of Shandong University of Science and Technology for Recruited Talents (Project # 2015RCJJ006). The authors also thank the editor and anonymous referees for their insightful comments, which improved this paper.

References

- [1] D. Fritsch, M. Rothermel, Oblique image data processing-potential, experiences and recommendations, in: Proc. 54th Photogrammetric Week, 2013.
- [2] N. Karbo, R. Schroth, Oblique aerial photography: a status review, in: Proc. 52nd Photogrammetric Week, 2009.
- [3] G. Petrie, Systematic oblique aerial photography using multiple digital cameras, *Photogrammetric Engineering & Remote Sensing* 75(2)(2009) 102-107.
- [4] V. Heikkinen, T. Tokola, J. Parkkinen, I. Korpela, Simulated multispectral imagery for tree species classification using support vector machines, *Geoscience and Remote Sensing* 48(3)(2009) 1355-1364.

- [5] B. Zhang, Z. Hu, K.F. Xing, Performance of RS-Turbo concatenated code in AOS, in: Proc. International Conference Electronic Measurement & Instruments (ICEMI), 2013.
- [6] F. Prandi, C. Achille, R. Brumana, F. Fassi, L. Fregonese, Lidar and Pictometry images integrated use for 3D model generation, in: J. Chen, J. Jiang, W.G. Kainz (Eds.), International Archives of the Photogrammetry, Remote Sensing and Spatial Information Sciences (IAPRS), Vol. XXXVII, Part B2, 3-11 July, Beijing, 2008, pp. 763-770.
- [7] L.R. Liu, J.Z. Zuo, G.J. Yue, R.C. Qu, Research on positioning and orienting methods of SWDC-5 oblique images, *Geomatics & Spatial Information Technology* 37(9)(2014) 6-9.
- [8] G. Le Besnerais, M. Sanfourche, F. Champagnat, Dense height map estimation from oblique aerial image sequences, *Computer Vision and Image Understanding* 109(2)(2008) 204-225.
- [9] G.J. Grenzdorffer, M. Guretzki, I. Friedlander, Photogrammetric image acquisition and image analysis of oblique imagery, *The Photogrammetric Record* 23(124)(2008) 372-386.
- [10] J. Hotle, Photogrammetric measurements in oblique aerial images, *Photogrammetrie, Fernerkundung, Geoinformation* (2008) 7-14.
- [11] A.P. Nyaruhuma, M. Gerke, G. Vosselman, Line matching in oblique airborne images to support automatic verification of building outlines, in: Proc. ASPRS 2010 Annual Conference, 2010.
- [12] J. Xiao, M. Gerke, G. Vosselman, Automatic detection of buildings with rectangular flat roofs from multi-view oblique imagery," in: N. Paparoditis, M. Pierrot-Deseilligny, C. Mallet, O. Tournaire (Eds.), International Archives of the Photogrammetry, Remote Sensing and Spatial Information Sciences (IAPRS), Vol. XXXVIII, Part 3A, 1-3 September 2010, Saint-Mandé, France, 2010, pp. 251-256.
- [13] M. Wang, H. Bai, F. Hu, Automatic texture acquisition for 3D model using oblique aerial images, in: Proc. Intelligent Networks and Intelligent Systems, 2008.
- [14] Y. D. Wang, S. Schultz, F. Giuffrida, Pictometry's proprietary airborne digital imaging system and its application in 3D city modeling, in: J. Chen, J. Jiang, J.A. Baudoin (Eds.), International Archives of the Photogrammetry, Remote Sensing and Spatial Information Sciences (IAPRS), Vol. XXXVII, Part B1, 3-11 July, Beijing, 2008, pp. 1065-1070.
- [15] E. Lagunnas, M.G. Amin, F. Ahmad, M. Najar, Pattern matching for building feature extraction, *Geoscience and Remote Sensing Letters* 11(2014) 2193-2197.
- [16] J.Y. Rau, C.Y. Chu, Vector-based occlusion detection for automatic facade texture mapping, in: Proc. Multi-Platform/Multi-Sensor Remote Sensing and Mapping (M2RSM), 2011.
- [17] X. Guo, X. Huang, L.P. Zhang, Three-dimensional wavelet texture feature extraction and classification for multi/hyperspectral imagery, *Geoscience and Remote Sensing Letters* 11(2014) 2183-2187.
- [18] H. Cheng, J.P. Zhang, An automatic method for texture extraction and mapping in 3d building reconstruction, in Proc. International Conference on Information and Automation (ICIA), 2012.
- [19] H.J. Luan, X.Q. Wang, Q.J. Tian, C.Z. Wei, Comparison of methods of fractal texture extraction for high-resolution remotely sensed images, in Proc. Earth Observation and Remote Sensing Applications (EORSA), 2012.
- [20] Z.J. Lin, F.F. Xie, G.Z. Su, Accuracy analysis of low altitude photogrammetry with wide-angle camera, *Acta Geodaetica et Cartographica Sinica* 43(10)(2014) 991-997.
- [21] D.L. Wang, J.H. Xiao, Y.C. Wang, Aerial route design approach for stereomapping based on stereomodel overlap, *Acta Geodaetica et Cartographica Sinica* 40(2)(2011) 188-192.
- [22] H.B. Pan, G.T. Zhang, M. Xin, Accuracy analysis and verification of ZY-3 products, *Acta Geodaetica et Cartographica*

Sinica 33(3)(2008) 102-105.

- [23] S.P. Ji, Y. Shi, Image matching and bundle adjustment using vehicle-based panoramic camera, *Acta Geodaetica et Cartographica Sinica* 42(1)(2013) 94-97.
- [24] C. Li, The necessary and sufficient condition of camera calibration and attitude determination based on vanishing points with their uncertainty analysis, *Acta Geodaetica et Cartographica Sinica* 41(6)(2012) 851-856.
- [25] Z.J. Lin, D.R. Li, Y.Y. Xu, General review on the new progress of earth observations, *Science of Surveying and Mapping* 36(4)(2011) 5-8.
- [26] Z.J. Lin, G.Z. Su, F.F. Xie, UAV borne low altitude photogrammetry system, *International Archives of the Photogrammetry*, in: M. Shortis, N. El-Sheimy (Eds.), *Remote Sensing and Spatial Information Sciences(IAPRS)*, Vol.XXXIX, Part B1, 25 August-1 September, Melbourne, Australia, 2012, pp. 415-423.